ChemComm

COMMUNICATION

View Article Online
View Journal

Published on 08 September 2016. Downloaded by University of California - San Diego on 18/09/2016 16:48:54.

Cite this: DOI: 10.1039/c6cc05992a

Received 21st July 2016,
Accepted 8th September 2016

DOI: 10.1039/c6cc05992a

www.rsc.org/chemcomm

Hierarchical silicalite-1 octahedra comprising highly-branched orthogonally-stacked nanoplates as efficient catalysts for vapor-phase Beckmann rearrangement†

Albert Chang,[a] Hsu-Ming Hsiao,[a] Tsai-Hsiu Chen,[a] Ming-Wen Chu[b] and Chia-Min Yang*[ac]

A triblock structure-directing agent was designed to synthesize hierarchical silicalite-1 octahedra comprising highly-branched, orthogonally-stacked and self-pillared nanoplates that exhibited excellent and stable activity for the vapor-phase Beckmann rearrangement of cyclic oximes and high lactam selectivity.

The development of zeolitic materials with hierarchical pore architectures is of great importance for heterogeneous catalysis and related applications.[1–5] Among the reported preparation methods,[6–13] direct synthesis using bifunctional structure-directing agents (SDAs) composed of spaced quaternary ammonium groups and long-chain alkyl groups for directing the formation of micropores and mesopores, respectively, is considered the most versatile and promising route to prepare hierarchical zeolites comprising stacked zeolite nanosheets or nanoporous zeolites.[11–13] The synthetic strategy has quickly attracted researchers to prepare a variety of SDAs with similar micropore-/mesopore-generating motifs to synthesize stacked MFI zeolite nanosheets.[14–17] The capability to further control the growth and stacking of zeolite nanosheets is crucial: not only may possible collapse of nanosheets after SDA removal be prevented, but more significantly, unique surface sites may be generated at the junctions of well-organized nanosheets. For example, the vapor-phase Beckmann rearrangement of cyclohexanone oxime into ε-caprolactam is a green process using pure-silica MFI zeolite (*i.e.* silicalite-1) as a solid acid catalyst.[18–21] The exposed silanol groups, especially the nest of silanol groups, are generally recognized as the active sites for this type of reaction.[18–21] For well-organized silicalite-1 nanosheets, the surface structure at nanosheet junctions may be unique and catalytically active for the reactions. Orthogonal stacking of zeolite nanosheets, a phenomenon probably related to the zeolite structure,[22] has sometimes been observed in the materials synthesized with bifunctional and other types of SDAs,[11–17,23–24] but the density of perpendicular junctions is too low to explore their catalytic properties. To date, the only material with high-density perpendicular nanosheet junctions has been synthesized by repetitive branching.[25]

We herein report a new design of the SDA that can direct the formation of hierarchical silicalite-1 octahedra comprising highly-branched, orthogonally-stacked and self-pillared nanoplates. The SDA (Scheme 1) features a tripropylene oxide (denoted PO_3) linker connecting two blocks of triquaternary (spaced by the $-C_6H_{12}-$ group) ammonium groups (denoted N_3). During zeolite synthesis, the short PO_3 linker of the SDA (C_6H_{13}–$N^+(CH_3)_2$–C_6H_{12}–$N^+(CH_3)_2$–C_6H_{12}–$N^+(CH_3)_2$–PO_3–$N^+(CH_3)_2$–C_6H_{12}–$N^+(CH_3)_2$–C_6H_{12}–$N^+(CH_3)_2$–C_6H_{13}($6OH^-$), abbreviated to N_3–PO_3–N_3) limits the relative degree of freedom of the two structure-directing N_3 blocks, thereby facilitating branching of MFI nanosheets. The material possessed a significant amount of silanol nest-like species, most likely at the perpendicular junctions of nanoplates, and showed excellent and stable activity of the vapor-phase Beckmann rearrangement and high lactam selectivity. The study demonstrates a new design rule of the SDA for preparing highly branched and self-pillared zeolite nanosheets for catalytic applications.

Hierarchical silicalite-1 octahedra were synthesized at 150 °C for 2 days using tetraethoxysilane as a silica source, N_3–PO_3–N_3 as an SDA, and sodium hydroxide as a base. The SDA was stable under the synthesis conditions, as indicated by the comparison of

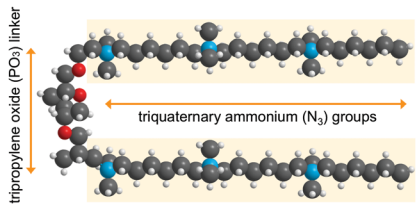

Scheme 1 Molecular structure of the N_3–PO_3–N_3 structure-directing agent.

[a] Department of Chemistry, National Tsing Hua University, Hsinchu 30013, Taiwan. E-mail: cmyang@mx.nthu.edu.tw
[b] Center for Condensed Matter Sciences, National Taiwan University, Taipei 10617, Taiwan
[c] Frontier Research Center on Fundamental and Applied Sciences of Matters, National Tsing Hua University, Hsinchu 30013, Taiwan

† Electronic supplementary information (ESI) available. See DOI: 10.1039/c6cc05992a

Published on 08 September 2016. Downloaded by University of California - San Diego on 18/09/2016 16:48:54.

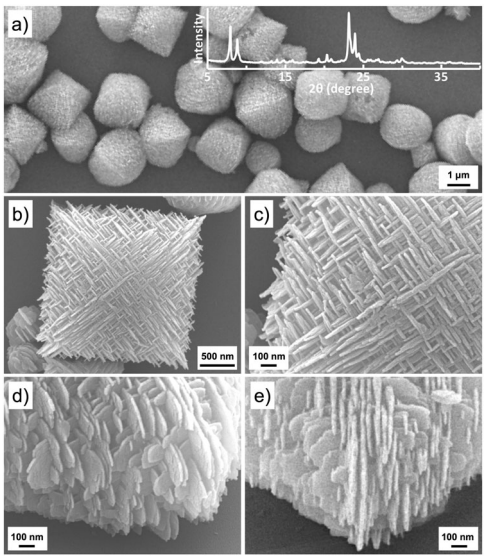

Fig. 1 (a–e) SEM images of hierarchical silicalite-1 octahedra. The PXRD pattern of the sample is also shown in (a).

the ^{13}C-NMR spectra of the SDA with that of the same SDA after heating at 150 °C for 2 days and with the solid-state ^{13}C CP/MAS NMR spectrum of the as-synthesized silicalite-1 material (Fig. S1 in the ESI†). Detailed synthesis procedures of N_3–PO_3–N_3 and silicalite-1 materials are given in the ESI.† Scanning electron microscopy (SEM) showed that the sample contains 2–3 μm particles with octahedral shape, and powder X-ray diffraction (PXRD) confirmed the formation of an MFI structure (Fig. 1a). The fact that only the *h*0*l* reflections are sufficiently sharp suggests the MFI nanosheets grow preferentially along the *a*–*c* planes.[11] Notably, each silicalite-1 octahedron is composed of ~15–30 nm-thick nanoplates that are oriented exclusively along two perpendicular directions and intersect one another to form a self-pillared architecture (Fig. 1b–e). Obviously, the density of perpendicular junctions in each octahedron is very high. The intergrown and orthogonally-stacked zeolitic nanoplates, together with nanoparticle aggregates, were observed after 38 h of hydrothermal synthesis (Fig. S2 in the ESI†).

The sample was calcined and crushed for high-resolution transmission electron microscopy (HRTEM) investigation. The image viewed across the thin dimension of a nanoplate (Fig. 2a) can be identified as the projection along the [010] axis of the MFI structure. The orthogonally connected nanoplates are not fully densely packed (Fig. 2a and b), thereby creating rectangular channels in the octahedra. Certainly, the channels should also exist in the as-synthesized sample, and this was confirmed by the presence of a H4-type hysteresis loop at a relative pressure of 0.47–0.95 in the nitrogen physisorption isotherm (Fig. 3a). Since the sudden decrease in the volume adsorbed along the desorption branch and a forced closure of the hysteresis loop may have originated from the tensile strength effect,[26] the adsorption branch of the isotherm was analyzed by the nonlocal density functional theory (NLDFT) method (by using the NLDFT–N_2–silica adsorption branch kernel). The analysis suggested that the rectangular channels vary in dimensions from about 3 to 9 nm

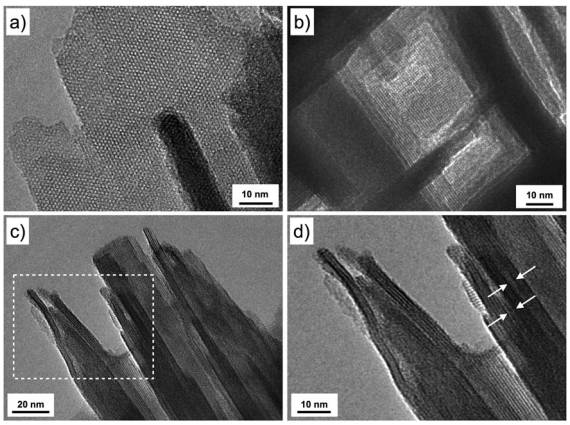

Fig. 2 (a–d) HRTEM images of hierarchical silicalite-1 octahedra.

(Fig. S3 in ESI†), and the surface area and total pore volume of the as-synthesized sample are 53 m^2 g^{-1} and 0.14 cm^3 g^{-1}, respectively. The HRTEM images in Fig. 2c and d further reveal that the nanoplates in the silicalite-1 octahedra are composed of parallel and spaced MFI nanosheets with a thickness of *ca.* 3 nm and the inter-sheet spacing is *ca.* 2 nm (indicated by arrows in Fig. 2d). In agreement with the observation, solid-state ^{29}Si MAS NMR shows that the $Q^3/(Q^3 + Q^4)$ ratio (Q^n: $(Si(OSi)_n(OH)_{4-n})$) of the as-synthesized sample is 25% (Fig. S4 in the ESI†), corresponding to a thickness of 1–1.5 unit cells along the *b* axis of the MFI structure (estimated based on the structure model constructed by Tsapatsis and coworkers for the same type of MFI nanosheet).[27]

We speculate that the short PO_3 linker in the triblock SDA plays an essential role in the formation of perpendicular nanosheet junctions in the hierarchical silicalite-1 octahedra. After an MFI-directing N_3 block of an SDA molecule is incorporated into an MFI

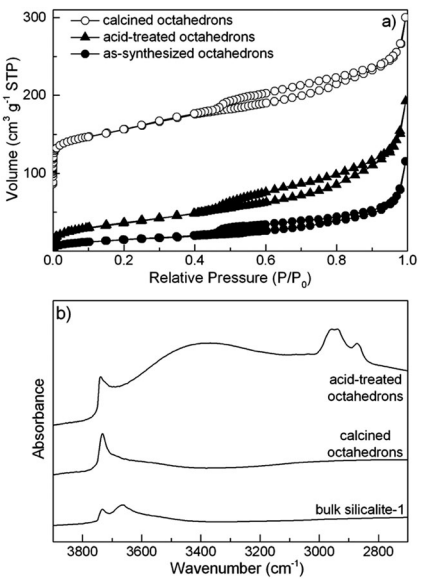

Fig. 3 (a) Nitrogen physisorption isotherms of the as-synthesized, acid-treated and calcined samples of hierarchical silicalite-1 octahedra. (b) FT-IR spectra of acid-treated and calcined silicalite-1 octahedra and calcined bulk silicalite-1 after dehydration at 400 °C.

 This journal is © The Royal Society of Chemistry 2016

Published on 08 September 2016. Downloaded by University of California - San Diego on 18/09/2016 16:48:54.

nanosheet growing preferentially along the *a*–*c* planes,[11] the other N_3 block of the same molecule may be incorporated either into the same nanosheet or into the adjacent one, with the former being least likely to happen due to the high strain of the molecular configuration. With a short PO_3 block to link each other, the adjacent nanosheet is forced to pack together at such a small length scale. Determined by both the configuration of N_3–PO_3–N_3 and the zeolite structure,[22] the nanosheets may be preferentially stacked parallel (corresponding to the least strained linear configuration of the SDA) or orthogonally (with perpendicularly aligned N_3 blocks) to each other. The parallel packed nanosheets eventually grow into nanoplates and the orthogonally connected ones create perpendicular junctions. The crucial role of the short linker in generating high-density perpendicular junctions was further supported by the fact that the synthesis using an SDA with a longer PO linker (N_3–PO_{33}–N_3) resulted in silicalite-1 particles comprising less branched and rather randomly stacked zeolite nanoplates (*cf.* Fig. S5 in the ESI†).

The hierarchical silicalite-1 octahedra possess three different types of pores, *i.e.* the rectangular channels created by orthogonally connected nanoplates, the spacing in between the parallel-stacked MFI nanosheets in the nanoplates, and the micropores in the nanosheets. The volume of each pore type was evaluated by nitrogen physisorption analysis (Fig. 3a and Fig. S3 in the ESI†). For the calcined octahedra exhibiting a surface area of 488 $m^2\ g^{-1}$ and a total pore volume of 0.43 $cm^3\ g^{-1}$, the zeolitic micropore volume is 0.18 $cm^3\ g^{-1}$ and the contribution from the rectangular channels is 0.16 $cm^3\ g^{-1}$ estimated from the value for the as-synthesized sample containing 15 wt% of the SDA (by deducting the weight of the SDA from the total sample weight; the TGA curve of the as-synthesized sample is shown in Fig. S6 in the ESI†). That leaves the volume of the inter-sheet spacing to be 0.09 $cm^3\ g^{-1}$. On the other hand, the inter-sheet spacing could be selectively vacated, without generating the zeolite micropores, by sulfuric acid treatment[28,29] to remove the PO_3 blocks of the SDA. Nitrogen physisorption analysis suggests that the acid-treated sample mainly contains pores with diameters larger than 2 nm (Fig. S3 in the ESI†) and the volume of the inter-sheet spacing is estimated to be 0.12 $cm^3\ g_{silica}^{-1}$. The difference in the values for the calcined (0.09 $cm^3\ g^{-1}$) and acid-treated (0.12 $cm^3\ g^{-1}$) samples suggests a minor degree of collapse of MFI nanosheets inside the nanoplates during calcination without causing a discernable morphological change (Fig. S7 in the ESI†). The calcination also led to further condensation of silanol groups, as indicated by a decreased $Q^3/(Q^3 + Q^4)$ ratio of 9%. Such a phenomenon was not seen for the acid-treated sample ($Q^3/(Q^3 + Q^4)$ = 25%) (Fig. S4 in the ESI†). Furthermore, more severe loss of silanol groups during calcination was observed for the hierarchical silicalite-1 octahedra than for the silicalite-1 nanosheets reported by Ryoo *et al.*[21] This may be reasonably speculated to be associated with the silanol condensation at nanoplate junctions. Fourier transform infrared (FT-IR) spectroscopy was further applied to corroborate the speculation. Fig. 3b compares the spectra of the dehydrated (at 400 °C in a vacuum for 12 h) samples of acid-treated and calcined silicalite-1 octahedra and bulk (calcined) silicalite-1[18] (see Fig. S8 in the ESI† for sample characterization). Interestingly, the acid-treated sample exhibited a relatively weak peak assignable to isolated (non-hydrogen-bonding) silanols (3740 cm^{-1}) and a strong absorption band centered at 3400 cm^{-1} which may be associated with the highly hydrogen-bonding silanol nest-like species.[18] The peaks of the remaining N_3 blocks were also observed at 2800–3000 cm^{-1}. On the other hand, the calcined sample mainly possessed isolated silanols and the amount is significantly less than that for the silicalite-1 nanosheets reported by Ryoo *et al.*[21] For comparison, the bulk silicalite-1 showed peaks mainly attributed to both isolated (3740 cm^{-1}) and vicinal (3680 cm^{-1}) silanols. The results strongly suggest the presence of silanol nest-like species in the acid-treated silicalite-1 octahedra that survived at a temperature as high as 400 °C.

With unique hierarchical porosity to facilitate mass transport and distinct silanol nest-like surface species, the acid-treated silicalite-1 octahedra were tested for vapor-phase Beckmann rearrangement. As expected, the sample exhibited high conversion of cyclohexanone oxime (CHO), high selectivity to ε-caprolactam (CL), and high catalytic stability. As shown in Fig. 4, the conversion of CHO was 95% at the beginning of the reaction, which decreased to 61% and became stable at an on-stream time of 45 h. Moreover, the selectivity to CL immediately increased from 80% to ~95% within the first hour and remained nearly unchanged afterwards. On the other hand, the calcined silicalite-1 octahedra showed similarly high CHO conversion (82% initially and decreased to 58% after 60 h) but much lower CL selectivity (~52%), with 5-hexenenitrile and cyclohexanone as main byproducts. For comparison, the reference bulk silicalite-1 catalyst exhibited an initial CHO conversion of 66% that decreased rapidly to 25% within 5 h, with CL selectivity kept at 48% during that period. The acid-treated sample of silicalite-1 particles comprising less branched and rather randomly stacked zeolite nanoplates (synthesized with N_3–PO_{33}–N_3) was found to possess fewer silanol nest-like species but more isolated silanols (*cf.* Fig. S5d in

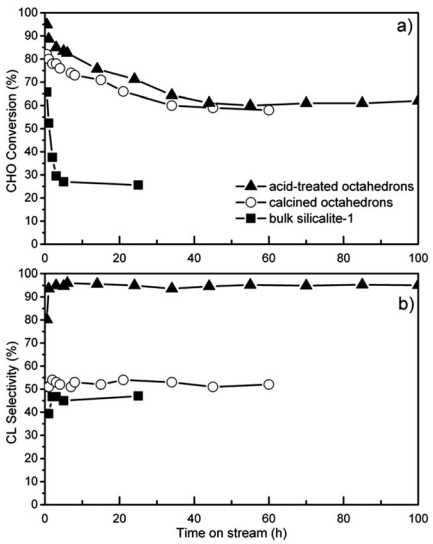

Fig. 4 Changes in CHO conversion (a) and CL selectivity (b) with on-stream time for the Beckmann rearrangement over silicalite-1 catalysts.

Published on 08 September 2016. Downloaded by University of California - San Diego on 18/09/2016 16:48:54.

the ESI†) and showed very similar high CHO conversion (92% initially and decreased to 60% after 45 h) but lower CL selectivity (70% initially, increased to ~80% within 10 h, and then remained at 80–83% afterwards) than the acid-treated hierarchical silicalite-1 octahedra did (Fig. S9 in the ESI†). A sample of solvent-extracted MCM-41 that is known to have a silanol-enriched mesopore surface[30,31] was also prepared and tested for the reaction. It gave an initial CHO conversion of 80% that promptly decreased to 50% within 5 h and then continuously decreased to 20% after an on-stream time of 60 h, and the CL selectivity remained in between 55 and 65% for most of the on-stream time (Fig. S10 in the ESI†). Obviously, the long catalytic lifetime of the calcined and acid-treated silicalite-1 octahedra comprising highly-branched and orthogonally-stacked nanoplates can be associated with the inherent hierarchical porosity to facilitate facile diffusion,[21] and the distinct behavior on the CL selectivity may be correlated with the type of catalytically active site, *i.e.* surface silanols, in the catalysts:[18,19,32,33] the isolated and vicinal silanol groups are the active sites for the calcined silicalite-1 octahedra, bulk silicalite-1 and solvent-extracted MCM-41, and the highly hydrogen-bonding silanol nest-like species, most likely at the perpendicular nanoplate junctions, may be responsible for the superior and stable catalytic activity of the acid-treated silicalite-1 octahedra. For the acid-treated silicalite-1 particles synthesized with N_3–PO_{33}–N_3, the presence of fewer silanol nest-like species may account for its lower CL selectivity than that for the acid-treated silicalite-1 octahedra. Interestingly, we found that the silicalite-1 octahedra could also catalyze the Beckmann rearrangement of cycloocatanone oxime (COO), an oxime that is larger than the micropore of the MFI zeolite.[20] Although both the calcined and acid-treated silicalite-1 octahedra showed a similar and relatively steady COO conversion of 15–20% after an on-stream time of 10 h, only the acid-treated sample produced the corresponding lactam with a selectivity of 65–75% (Fig. S11 in the ESI†). The results clearly indicate that the unique, silanol nest-like species in the acid-treated silicalite-1 octahedra are catalytically active for the vapor-phase Beckmann rearrangement reactions.

The reusability of the acid-treated silicalite-1 octahedra for the rearrangement of CHO into CL was also examined (detailed conditions provided in the ESI†). After the first cycle of the catalytic test, the regenerated sample still exhibited very high (~95%) and stable CL selectivity but gave a lower initial CHO conversion of 80% that gradually decreased to 41% and became stable (Fig. S12 in the ESI†). The catalytic performance remained nearly unchanged in the third and fourth catalytic cycles. The decreased catalytic activity seemed to correlate with the decreased amount of silanol species as evidenced by solid-state ^{29}Si MAS NMR (showing a decrease of the $Q^3/(Q^3 + Q^4)$ ratio from 25% for the acid-treated sample to 13%) and FT-IR (Fig. S13a and b in the ESI†). The recycled silicalite-1 octahedra did not show discernable structural and morphological changes (Fig. S13c and d in the ESI†).

In summary, we have designed a new type of triblock SDA for the direct synthesis of hierarchical silicalite-1 octahedra with highly-branched and self-pillared nanoplates. The orthogonal stacking of nanoplates is associated with the formation of silanol nest-like species at the junction of nanoplates. The hierarchical silicalite-1 octahedra exhibited excellent and stable activity for the vapor-phase Beckmann rearrangement and high lactam selectivity. The results demonstrate a new design rule of the SDA for preparing novel hierarchical zeolites for catalytic and other applications.

The authors thank the Ministry of Science and Technology of Taiwan for the financial support under contract MOST 103-2628-M-007-006-MY3.

Notes and references

1 J. Cejka and S. Mintova, *Catal. Rev.: Sci. Eng.*, 2007, **49**, 457.
2 A. Corma, M. Diaz-Cabanas, J. Martinez-Triguero, F. Rey and J. Rius, *Nature*, 2002, **418**, 514.
3 M. E. Davis, *Nature*, 2002, **417**, 813.
4 W. Vermeiren and J. P. Gilson, *Top. Catal.*, 2009, **52**, 1131.
5 X. Xu, J. Wang and Y. Long, *Sensors*, 2006, **6**, 1751.
6 A. H. Janssen, A. J. Koster and K. P. de Jong, *Angew. Chem., Int. Ed.*, 2001, **40**, 1102.
7 V. Valtchev, G. Majano, S. Mintova and J. Perez-Ramirez, *Chem. Soc. Rev.*, 2013, **42**, 263.
8 M. W. Anderson, S. M. Holmes, N. Hanif and C. S. Cundy, *Angew. Chem., Int. Ed.*, 2000, **39**, 2707.
9 M. Choi, H. S. Cho, R. Srivastava, C. Venkatesan, D. H. Choi and R. Ryoo, *Nat. Mater.*, 2006, **5**, 718.
10 H. Wang and T. J. Pinnavaia, *Angew. Chem., Int. Ed.*, 2006, **45**, 7603.
11 M. Choi, K. Na, J. Kim, Y. Sakamoto, O. Terasaki and R. Ryoo, *Nature*, 2009, **461**, 246.
12 K. Na, C. Jo, J. Kim, K. Cho, J. Jung, Y. Seo, R. J. Messinger, B. F. Chmelka and R. Ryoo, *Science*, 2011, **333**, 328.
13 W. Park, D. Yu, K. Na, K. E. Jelfs, B. Slater, Y. Sakamoto and R. Ryoo, *Chem. Mater.*, 2011, **23**, 5131.
14 B. Y. Liu, Q. Q. Duan, C. Li, Z. H. Zhu, H. X. Xi and Y. Qian, *New J. Chem.*, 2014, **38**, 4380.
15 R. Kore, R. Srivastava and B. Satpati, *Chem. – Eur. J.*, 2014, **20**, 11511.
16 D. D. Xu, Y. H. Ma, Z. F. Jing, L. Han, B. Singh, J. Feng, X. F. Shen, F. L. Cao, P. Oleynikov, H. Sun, O. Terasaki and S. N. Che, *Nat. Commun.*, 2014, **5**, 4262.
17 D. D. Xu, Z. F. Jing, F. L. Cao, H. Sun and S. N. Che, *Chem. Mater.*, 2014, **26**, 4612.
18 G. P. Heitmann, G. Dahlhoff and W. F. Holderich, *J. Catal.*, 1999, **186**, 12.
19 A. B. Fernandez, A. Marinas, T. Blasco, V. Fornes and A. Corma, *J. Catal.*, 2006, **243**, 270.
20 H. Ichihashi, M. Ishida, A. Shiga, M. Kitamura, T. Suzuki, K. Suenobu and K. Sugita, *Catal. Surv. Asia*, 2003, **7**, 261.
21 J. Kim, W. Park and R. Ryoo, *ACS Catal.*, 2011, **1**, 337.
22 I. Díaz, E. Kokkoli, O. Terasaki and M. Tsapatsis, *Chem. Mater.*, 2004, **16**, 5226.
23 W. Chaikittisilp, Y. Suzuki, R. R. Mukti, T. Suzuki, K. Sugita, K. Itabashi, A. Shimojima and T. Okubo, *Angew. Chem., Int. Ed.*, 2013, **52**, 3355.
24 G. Bonilla, I. Díaz, M. Tsapatsis, H.-K. Jeong, Y. Lee and D. G. Vlachos, *Chem. Mater.*, 2004, **16**, 5697.
25 X. Y. Zhang, D. X. Liu, D. D. Xu, S. Asahina, K. A. Cychosz, K. V. Agrawal, Y. Al Wahedi, A. Bhan, S. Al Hashimi, O. Terasaki, M. Thommes and M. Tsapatsis, *Science*, 2012, **336**, 1684.
26 J. C. Groen, L. A. A. Peffer and J. Pérez-Ramírez, *Microporous Mesoporous Mater.*, 2003, **60**, 1.
27 K. Varoon, X. Y. Zhang, B. Elyassi, D. D. Brewer, M. Gettel, S. Kumar, J. A. Lee, S. Maheshwari, A. Mittal, C. Y. Sung, M. Cococcioni, L. F. Francis, A. V. McCormick, K. A. Mkhoyan and M. Tsapatsis, *Science*, 2011, **334**, 72.
28 C.-M. Yang, B. Zibrowius, W. Schmidt and F. Schüth, *Chem. Mater.*, 2004, **16**, 2918.
29 C.-M. Yang, B. Zibrowius, W. Schmidt and F. Schüth, *Chem. Mater.*, 2003, **15**, 3739.
30 N. Lang and A. Tuel, *Chem. Mater.*, 2004, **16**, 1961.
31 C.-J. Lin, S.-H. Huang, N.-C. Lai and C.-M. Yang, *ACS Catal.*, 2015, **5**, 4121.
32 Y. Izumi, H. Ichihashi, Y. Shimazu, M. Kitamura and H. Sato, *Bull. Chem. Soc. Jpn.*, 2007, **80**, 1280.
33 G. Dahlhoff, J. P. M. Niederer and W. F. Hoelderich, *Catal. Rev.: Sci. Eng.*, 2001, **43**, 381.

 This journal is © The Royal Society of Chemistry 2016